Nonlinear Krylov acceleration for CFD-based Aeroelasticity

Zhengkun Feng[1,†], Azzeddine Soulaïmani[1,‡], and Yousef Saad[2,§]

[1] *Department of Mechanical Engineering, École de Technologie Supérieure, 1100 rue Notre-Dame Ouest, Montreal(QC), H3C 1K3, Canada;*
[2] *Department of Computer Science and Engineering, University of Minnesota, 4-192 EE/CS Building, 200 Union Street S. E., Minneapolis, MN 55455.*

Abstract

A nonlinear computational aeroelasticity model based on the Euler equations of compressible flows and the linear elastodynamic equations for structures is developed. The Euler equations are solved on dynamic meshes using the ALE kinematic description. Thus, the mesh constitutes another field governed by pseudo-elatodynamic equations. The three fields are discretized using proper finite element formulations which satisfy the geometric conservation law. A matcher module is incorporated for the purpose of pairing the grids on the fluid-structure interface and for transferring the loads and displacements between the fluid and structure solvers. Two solutions strategies (Gauss Seidel and Schur-Complement) for solving the nonlinear aeroelastic system are discussed. Using second order time discretization schemes allows us to use large time steps in the computations. The numerical results on the AGARD 445.6 aeroelastic wing compare well with the experimental ones and show that the Schur-complement coupling algorithm is more robust than the Gauss-Seidel algorithm for relatively large oscillation amplitudes.

Key words: Aeroelasticity; Fluid-structure interaction; Coupling; Simulation; Transonic flow; Nonlinearity; Gauss Seidel, Schur-Complement, Krylov algorithms.

1 INTRODUCTION

Multi-physics problems represent a large class of applications. The study of fluid-structure interactions in aerodynamics, the thermo-mechanical coupling problem of turbo-machines and the vibro-aeroacoustic problems are some relevant engineering examples. Because the solution to these problems requires the coupling of equations from different engineering fields, this cross-disciplinary coupling increases the computational load and the complexity of computational procedures. Transonic airflows around a flexible structure is characterized by the existence of nonlinearities, such as shock waves and flow induced vibrations [1]. In the classical linear aeroelasticity theory [2,3], airflow is assumed inviscid, incompressible and irrotational. Corresponding numerical methods can be found in the early literature, such as the well-known Doublet Lattice method, the Vortex-Lattice method, the panel method and the transonic-small-disturbance (TSD) method. However, the linear theory cannot accurately predict the transonic dip [4], therefore nonlinear aeroelasticity theories are required. Discussions on the behaviors of the aerodynamic nonlinearity can be found in Ref. [5]. The full-potential equation, which describes the nonlinearity of a transonic flow, gives better solutions [6] when the shock is weak. But for flows with strong shocks, a high order model such

[1] Correspondence to: A. Soulaïmani, Département de Génie Mécanique, École de technologie supérieure; 1100 Notre-Dame Ouest, Montréal (Québec), H3C 1K3, Canada. Tel : +15143968977; Fax : +15143968530
[†]E-mail:Feng.Zhengkun@etsmtl.ca
[‡]E-mail: Azzeddine.Soulaimani@etsmtl.ca. Work supported by NSERC and CRIAQ grants.
[§]E-mail: saad@cs.umn.edu. Work supported by NSF grant ACI-03055120 and by the Minnesota Supercomputer Institute.
An earlier version of this paper was presented in the 7th FSI, AE & FIV+N Symposium, held within the 2006 PV & P Conference in Vancouver, BC, Canada

as the Euler equations that describe more completely the nonlinearity in transonic regime are required to obtain accurate solutions [7,8]. Indeed, the computational cost increases evidently.

In this paper, the aeroelastic system is modeled by coupling numerically three fields, which are respectively the structural, the fluid, and the mesh fields, through an information transfer module. We assume that the flow is described by the Euler equations and the structure is modeled by the linear elastodynamic equations. The nonlinear coupling between the structure and the fluid is enforced by imposing kinematic and dynamic compatibility conditions at the fluid-structure interface(FSI). The outline of the following sections is as follows : The governing equations of the complete system will be presented, followed by a description of the coupling algorithms and then a discussion of numerical results. The paper will end with concluding remarks.

2 AEROELASTICITY PROBLEM

Aeroelasticity is one of the most important and challenging examples of multi-physics applications. It couples two nontrivial applications and is characterized by multi-scale phenomena, both in time and space. The efficient solution to this problem is of critical importance to the design of aircrafts. The coupling between the fluid flow and the flexible structure displacement can produce instabilities that may compromise structural integrity. The flutter is a dynamical instability phenomenon exhibited by a flexible structure under the effect of high flow speed. It is thus crucial to ensure the aeroelastic stability of the flexible structure especially for structures used as aeronautic components.

2.1 Governing equations

Equations for the structure. The displacement $\mathbf{u}^s$ of a flexible elastic structure satisfies the dynamic equilibrium equations:

$$\rho_s {u^s}_{i,tt} + \sigma^s_{ij,j}(\mathbf{u}^s) = g_i \quad in \quad \Omega_s \tag{1}$$

where ρ_s is the structure density and $\sigma^{\mathbf{s}}$ is the Cauchy stress tensor. We assume an elastic material of the structure and small structural deformations. Thus, the constitutive relation between the Green strain tensor $\epsilon^{\mathbf{s}}$ and the Cauchy stress tensor reads $\sigma^{\mathbf{s}} = \mathbf{C}^s.\epsilon^{\mathbf{s}}$, with $\mathbf{C}^s$ the fourth order constitutive tensor of the structural material and $\epsilon^s_{ij,j} = \frac{1}{2}(u^s_{i,j} + u^s_{j,i})$. The structure is subjected to external forces and initial conditions. Particularly, kinematic and dynamic compatibility conditions at the fluid-structure interface Γ_{fs} should be respected.

Equations for the fluid. We consider that the fluid flow is modeled by the compressible Euler equations. These are written in a moving frame of reference(i.e. moving mesh) [9,10] and in terms of the conservative variables $\mathbf{U} = \rho(1, \mathbf{u}, e + \|\mathbf{u}\|^2/2)^T$ as:

$$\mathbf{U}_{,\mathbf{t}} + \mathbf{w}_i \mathbf{U}_{,i} + \mathbf{F}_{i,i} = 0 \quad in \quad \Omega_f \tag{2}$$

where ρ is the fluid density, $\mathbf{u} = \{u_i\}$ is the fluid velocity, p the pressure, e the total energy per unit mass, $\mathbf{F}_i = u_i\mathbf{U} + p(0, \delta_{\mathbf{i}}, u_i)^T$ is the convective flux in the ith direction, $\delta_i = \{\delta_{ij}\}$ is the Kronecker delta and $\mathbf{w} = \{w_i\}$ is the mesh velocity.

Compatibility conditions at the fluid-structure interface. Since the fluid is assumed non-viscous, the interface is a *slip* material boundary. This means that we have the following kinematic boundary condition along Γ_{fs}: $(\mathbf{u} - \mathbf{u}^{\mathbf{s}}_{,\mathbf{t}}).\mathbf{n}^{\mathbf{s}} = 0$ with $\mathbf{n}^{\mathbf{s}}$ is the unit normal vector at Γ_{fs}. The force acting on the structure is due to the fluid pressure. Thus, we have the dynamic compatibility conditions along the interface: $\sigma^s_{ij}\ n^s_j = -p\ n^s_i$.

Equations for the mesh movement. The mesh of the fluid domain is animated with its own motion so as to fulfill the kinematical compatibility constraints (i.e., to preserve the fact that the interface is a material boundary) and to maintain the quality of the discretization. This can be done by solving an elliptic problem for the mesh displacement $\mathbf{u}^{\mathbf{m}}$ [10]. At the fluid-structure interface (FSI) the mesh displacement is imposed to that of the structure. In the

following, we assume that the mesh represents an isotropic elastic material. Its motion is assumed to be governed by the elastodynamic equations:

$$\rho_m {u^m}_{i,tt} + \sigma^m_{ij,j}(\mathbf{u^m}) = 0 \quad in \quad \Omega_f \tag{3}$$

where ρ_m is the fictitious mesh density and $\sigma^{\mathbf{m}}$ is the Cauchy stress tensor. The mesh velocity is given by $\mathbf{w} = \mathbf{u^m}_{,t}$. The boundary conditions are : $\mathbf{u^m} = \mathbf{u^s}$ at Γ_{fs} and zero elsewhere. We denote by $\mathbf{F}^m$ the deformation tensor of the mesh movement, i.e. $F^m_{ij} = \delta_{ij} + u^m_{i,j}$. The mesh deformations are not assumed to be small, so the Green strain tensor $\mathbf{E}^m$ is given by $\mathbf{E}^m = \frac{1}{2}(\mathbf{F^m}^T\mathbf{F^m} - \mathbf{I})$. Thus the constitutive relation between the Green strain tensor $\mathbf{E}^m$ and the second Piola-Kirchoff stress tensor $\mathbf{S}^m$ reads: $\mathbf{S}^m = \mathbf{C}^m\mathbf{E}^m$, with $\mathbf{S}^m = J\ \mathbf{F^m}^{-1}\sigma^m\mathbf{F^m}^{-T}$, $J = det(\mathbf{F^m})$ and $\mathbf{C}^m$ the fictitious fourth order tensor for the mesh material.

2.2 Space discretizations

Finite elements for the structure. The equilibrium equations for the structure and for the mesh are discretized using a classical weak variational formulation and finite element interpolations (three-dimensional continuum elements for the mesh, and structural elements such as shells, solids, beams and trusses). The discrete sets of equations for the structure are written in the matrix form as:

$$\mathbf{M}^s\{\mathbf{U}^s\}_{,tt} + \mathbf{K}^s\{\mathbf{U}^s\} = \{\mathbf{G}^s(p_{fs})\} \tag{4}$$

with $\{\mathbf{U}^s\}$ is the set of structural degrees of freedom. Note that by introducing the dynamic boundary conditions at the fluid-structure interface, the right-hand side of (4) is dependent on the fluid pressure. The linear time-dependent system (4) can be solved using a direct time-stepping approach or by using a modal superposition analysis. We adopt the latter approach. Thus, equations (4) are transformed into a set of m ordinary differential equations where the unknown is the generalized modal displacement vector $\{\mathbf{Z(t)}\}$:

$$\{\mathbf{Z}\}_{,tt} + \mathbf{\Lambda}\{\mathbf{Z}\} = \{\mathbf{g}^s(p_{fs})\} \tag{5}$$

where $\mathbf{\Lambda} = diag(\omega_1^2, ..., \omega_m^2)$, ω_i^2 are the m-eigenvalues of the problem: $\mathbf{K}^s\{\phi_i\} = \omega_i^2\mathbf{M}^s\{\phi_i\}$ and ϕ_i are the eigenvectors. The vector of nodal displacements $\{\mathbf{U}^s\}$ is related to $\{\mathbf{Z}\}$ by $\{\mathbf{U}^s\} = \Phi\{\mathbf{Z}\}$ with $\Phi = [\phi_1, ..., \phi_m]$ and $\{\mathbf{g}^s\} = \Phi^T\{\mathbf{G}^s\}$.

Finite elements for the fluid. The space discretization of the Euler equations is made using the Stream-Line-Petrov-Galerkin method [11,12]. Consider a partition of the fluid domain into elements Ω^e. The SUPG formulation reads: find $\mathbf{U}$ such that for all weighting functions $\mathbf{W}$,

$$\sum_e \int_{\Omega^e} (\mathbf{W} + (\mathbf{A}_i^t\mathbf{W}_{,i}) \cdot \tau) \cdot (\mathbf{U}_{,t} + \mathbf{w}_{i,i}\mathbf{U} + \mathbf{F}_{i,i})\ d\Omega\ + \sum_e \int_{\Omega^e} \nu^e \mathbf{W}_{,i}\mathbf{U}_{,j}\ d\Omega = 0 \tag{6}$$

and with $\mathbf{A}_i = \partial F_i/\partial\mathbf{U}$ is the Jacobian matrix of the convective flux, ν^e is a positive coefficient dependent on the local residual vector $\mathbf{R} = (\mathbf{U}_{,t} + \mathbf{w}_{i,i}\mathbf{U} + \mathbf{F}_{i,i})$, and the matrix τ is commonly referred to as the matrix of time scales [11–13]. The SUPG formulation is built as a combination of the standard Galerkin integral form and a perturbation-like integral form depending on the local residual vector. The objective is to reinforce the stability inside the elements. The FE approximation of the variational formulation (6) uses linear piecewise polynomials over tetraedral elements. The discrete system corresponding to (6) is written in the form:

$$\mathbf{M}^f\{\mathbf{U^f}\}_{,t} + \mathbf{K}^f(\{\mathbf{U}^f\}, \{\mathbf{W}^f\})\{\mathbf{U}^f\} = \{\mathbf{G}^f\} \tag{7}$$

with $\{\mathbf{U^f}\}$ the set of the fluid nodal degrees of freedom, $\mathbf{M}^f$ is the fluid mass matrix and $\mathbf{K}^f$ is the stiffness matrix of the fluid. Since theses matrices and the right-hand side of (6) are obtained by an integration over a moving domain (then unknown domain), they are implicitly dependent on the structural displacement $\{\mathbf{U}^s\}$. Thus, there is a two-way coupling between the structure, the fluid and the moving mesh fields.

Finite elements for the mesh. A standard Galerkin variational formulation is established to solve (3). The corresponding discrete set of equations for the mesh are written in matrix form as:

$$\mathbf{M}^m\{\mathbf{U}^m\}_{,tt} + \mathbf{K}^m(\{\mathbf{U}^m\})\{\mathbf{U}^m\} = \{\mathbf{G}^m(\{\mathbf{U}\}^s)\} \tag{8}$$

with $\{\mathbf{U}^m\}$ is the set of mesh nodal degrees of freedom. Since the density ρ_m can be chosen arbitrarily, we set it to zero. Thus, (8) becomes a nonlinear steady problem. In order to avoid large distortions of small elements as the interface moves, the constitutive material properties of the mesh are chosen in the form $\mathbf{C}^m \simeq \mathbf{I}/|\Omega^e|$, where $|\Omega^e|$ is the volume of the corresponding element. Linear FE approximations over tetraedral elements are used.

2.3 Time discretizations

Implicit time marching schemes enable the use of large time steps for the structure as well as for the mesh and fluid fields. We adopt the trapezoidal rule (Newmark scheme) to integrate (5). At the time step $n+1$, one must solve:

$$Z_i^{(n+1)} = \frac{\Delta t^2/4}{1+\omega_i^2\Delta t^2/4}\Big(g^s(p_{fs})^{(n+1)} + \frac{1}{4\Delta t}[\frac{Z_i^n}{\Delta t} + \dot{Z}_i^n + \frac{\Delta t}{4}\ddot{Z}_i^n]\Big) \tag{9}$$

with $\dot{Z}_i^n = 2(Z_i^n - Z_i^{n-1})/\Delta t - \dot{Z_i^{n-1}}$, $\ddot{Z}_i^n = 4(Z_i^n - Z_i^{n-1})/\Delta t^2 - 4\dot{Z_i^{n-1}}/\Delta t - \ddot{Z^{n-1}}_i$, and Δt is the time step.

For the fluid, we choose an implicit scheme where the time derivative is approximated by a second-order backward difference scheme,

$$\{\mathbf{U}^f\}_{,t} \simeq (3\{\mathbf{U^{f,n+1}}\} - 4\{\mathbf{U^{f,n}}\} - \{\mathbf{U^{f,n-1}}\})/(2\Delta t)$$

Inserting this approximation into (7) leads to a nonlinear system for the fluid d.o.f. at each time step. This system as well as (8) is solved by a Newton-GMRES iterative algorithm [14].

2.4 Fluid-structure interface

A major stumbling block here is that the mesh for the fluid and the one for the structure do not match. A mechanism must be incorporated to make the correspondence when moving from the fluid to structure solves (Figure 1). In particular, compatibility conditions must be guaranteed on the interface between fluid and the structure [15–17]. Since nodes on both sides of the interface do not need to match, a search algorithm is used to identify the structure element that contains the fluid node. Once this mapping is obtained, local pressure forces are computed at each fluid interface node and then interpolated at the structure interface nodes. The resulting pressure load is used as a boundary condition for the structure. As the structure moves, the displacements of the fluid nodes at the interface are obtained by simple interpolation. These are then used as boundary conditions for the mesh solver. The grid velocity is computed for each fluid node and the kinematic boundary conditions at the interface are updated.

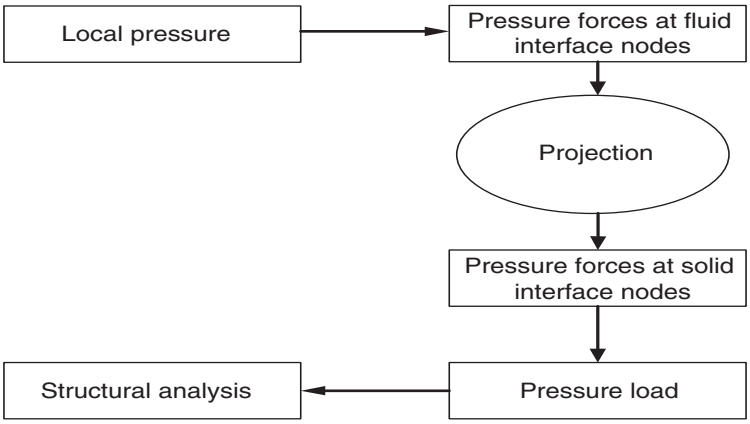

Fig. 1. Fluid-Structure data exchange

3 SOLUTION METHODS

The nonlinear aeroelasticity model describing the coupling (Fig. 1) of the fluid, mesh and structure fields can be presented in the following form [18]:

$$\left\{ \begin{array}{l} \mathbf{R}_1(\mathbf{Y}, \mathbf{Z}(p_{fs})) \\ \mathbf{R}_2(\mathbf{Y}, \mathbf{Z}(p_{fs})) \end{array} \right\} = 0 \tag{10}$$

where $\mathbf{Y}$ is the set of fluid and mesh variables which consist of vectors $\mathbf{U}^f$ and $\mathbf{u}^m$, $\mathbf{Z}(p_{fs})$ is the set of structural variables, p_{fs} is the pressure at the fluid-structure interface, $\mathbf{R}_1$ and $\mathbf{R}_2$ are the nonlinear discrete residuals of the fluid, mesh and structural variables, respectively.

The above coupled system can be formulated as a system of nonlinear equations:

$$F(\mathbf{U}) = 0; \quad \text{with} \quad U = \begin{pmatrix} \mathbf{Y} \\ \mathbf{Z} \end{pmatrix} \tag{11}$$

One can think of several approaches for solving the system (10) or (11). The first approach that comes to mind is to linearize the system and use a Newton-type method. The linear system resulting from the linearization would be,

$$\mathbf{K}_T \begin{pmatrix} \delta\mathbf{Y} \\ \delta\mathbf{Z}(p_{fs}) \end{pmatrix} = - \begin{pmatrix} \mathbf{R}_1(\mathbf{Y}, \mathbf{Z}(p_{fs})) \\ \mathbf{R}_2(\mathbf{Y}, \mathbf{Z}(p_{fs})) \end{pmatrix} \tag{12}$$

where $\mathbf{K}_T$ is the tangent matrix, formally written as:

$$\mathbf{K}_T = \begin{bmatrix} \mathbf{A} & \mathbf{C} \\ \mathbf{D} & \mathbf{B} \end{bmatrix} \tag{13}$$

A major difficulty with this "fully-coupled" approach is that the coupling sub-matrices $\mathbf{C}$ and $\mathbf{D}$ are not practically available. Indeed, they are difficult to express analytically and their approximation by some approximate differencing formulas would end-up being too costly.

An alternative which does not require Jacobians explicitly is to use a nonlinear Generalized Minimal Residual (GMRES) procedure to solve the system of nonlinear equations $F(\mathbf{U}) = 0$, see, e.g., [19–21]. Given the current iterate $\mathbf{U}_n$, we seek a new iterate $\mathbf{U}_{n+1} = \mathbf{U}_n + \delta_n$, where δ_n is in some subspace to be defined shortly. Ideally we wish to minimize $\|F(\mathbf{U}_n + \delta_n)\|_2$ over this subspace. This is a nonlinear optimization problem which is best solved by using a linear model. Specifically, an approximate solution is obtained by seeking to minimize instead $\|F(\mathbf{U}_n) + J_n\delta_n\|_2$ where J_n is the Jacobian matrix of F at the point $\mathbf{U}_n$. If we were able to solve the linear system $J\delta_n = -F(\mathbf{U}_n)$ exactly in the selected subspace this would just lead to a standard Newton step. A natural idea is to take an *approximate Newton step* which corresponds to selecting the Krylov subspace $K_m = \{v_1, J_n v_1, \cdots, J_n^{m-1} v_1\}$ where J_n is the Jacobian matrix of F at the point $\mathbf{U}_n$ and $v_1 = -F(\mathbf{U}_n)/\|F(\mathbf{U}_n)\|_2$. This amounts to an inexact Newton iteration where each linear system is approximated by m steps of the (linear) GMRES algorithm. It is also possible to add a backtracking strategy, see, e.g., [19] to improve global convergence.

The Nonlinear GMRES algorithm is sketched below. Note that the algorithm only requires the Jacobian matrix J in the form of matrix-vector produtcs in Line 6. Even when the Jacobian is not explicitly available, this product can be performed by a finite difference formula, such as,

$$J.v \approx \frac{F(\mathbf{U} + \epsilon v) - F(\mathbf{U})}{\epsilon} \ . \tag{14}$$

Note that this requires one residual evaluation per nonlinear loop (Lines 2 to 15) since $F(\mathbf{U})$ does not change throughout this loop and it can be saved.

Algorithm 1: Nonlinear GMRES

1. **Start:** Choose initial $\mathbf{U}$ and a dimension m of the Krylov subspace.
2. **Arnoldi process:**
3. Compute $\beta = \|F(\mathbf{U})\|_2$
4. and $v_1 = -F(\mathbf{U})/\beta$.
5. For $j = 1, 2, .., m$ do:
6. Compute Jv_j (where J = Jacobian of F at $\mathbf{U}$)
7. $h_{i,j} = (Jv_j, v_i), i = 1, 2, ..., j,$
8. $\hat{v}_{j+1} = Jv_j - \sum_{i=1}^{j} h_{i,j} v_i$
9. $h_{j+1,j} = \|\hat{v}_{j+1}\|_2$ and $v_{j+1}\hat{v}_{j+1}/h_{j+1,j}$
10. EndDo
11. Define the $(m+1) \times m$ matrix $\bar{H}_m\{h_{ij}$ if $i \leq j+1,$ 0 otherwise$\}$
12. and $V_m \equiv [v_1, v_2, \ldots v_m]$
13. **Form the approximate solution:** Find y_m the minimizer of
14. $\phi(y) \equiv \|\beta e_1 - \bar{H}_m y\|_2$, where $e_1 = [1, 0, \ldots 0]^T$.
15. Compute $\delta = V_m y_m$ and $\mathbf{U}_{n+1} = \mathbf{U}_n + \delta$.
16. **Backtrack:** Choose a damping scalar $\lambda \leq 1$ such that
17. $\|F(\mathbf{U} + \lambda\delta)\|_2$ decreases sufficiently relative to $\|F(\mathbf{U})\|_2$.
18. **Restart:** If satisfied stop, else set $\mathbf{U} \leftarrow \mathbf{U} + \lambda\delta$, $n \leftarrow n + 1$, and goto (2).

3.1 Nonlinear Block-Jacobi

When the mapping F is linear, i.e, when it is of the form $F(\mathbf{U}) = b - K * \mathbf{U}$, then the algorithm just given would be equivalent to a standard GMRES method for solving the system $K\mathbf{U} = b$, without preconditioning. One possibility of preconditining is to use a block-Jacobi approach which consists of defining the preconditioner as the matrix obtained from neglecting the coupling submatrices C, D in (13):

$$[\mathbf{M}] = \begin{bmatrix} \mathbf{A} & 0 \\ 0 & \mathbf{B} \end{bmatrix} \tag{15}$$

Note that in contrast with the coupling matrices $\mathbf{C}, \mathbf{D}$, the subbloks $\mathbf{A}$ and $\mathbf{B}$ are readily available.

Another intrepretation of the resulting procedure, is that the nonlinear GMRES algorithm is attempting to accelerate a secant-Newton procedure of the form

$$\begin{pmatrix} \mathbf{Y}_{new} \\ \mathbf{Z}_{new} \end{pmatrix} = \begin{pmatrix} \mathbf{Y} \\ \mathbf{Z} \end{pmatrix} - \begin{pmatrix} \mathbf{A}^{-1}\mathbf{R}_1(\mathbf{Y}, \mathbf{Z}(p_{fs})) \\ \mathbf{B}^{-1}\mathbf{R}_2(\mathbf{Y}, \mathbf{Z}(p_{fs})) \end{pmatrix} \tag{16}$$

The resulting procedure essentially solves equation (12) iteratively by replacing the tangent matrix $\mathbf{K}_T$ by the block diagonal matrix (15).

3.2 Nonlinear Gauss-Seidel algorithm

We next consider two alternative iterative schemes. The first is a nonlinear Gauss-Seidel iteration whereby the solution of the CFD solver at instant t^{n+1} is computed with the assumption that the solution of the CSD solver at the same step is already known and vice versa, for the solution of the CSD solver. Under well-known conditions [22, chap. 10] this iteration will be contracting [22, chap. 12] in some domain D, so that it will converge to a unique fixed point for any initial guess in the domain D. At the limit the coupling is 'consistent', in the sense that the pair of solutions found will satisfy both equations at the same time. The overall convergence rate is conditioned by the time step used and the magnitude of the motion. Though the analysis in [22] is for the scalar SOR-Newton iteration, it is generalizable to a block-SOR case. Recall that the case $\omega = 1$ corresponds to the (Block) Gauss-Seidel iteration. This algorithm is summarized next.

Algorithm 2: Nonlinear Block Gauss-Seidel iteration

1. Loop over time steps:
2. Until convergence Do:
3. Update the fluid field using the new boundary conditions.
4. Project fluid forces on the structure.
5. Update the structure displacements.
6. Update the mesh configuration using the new interface positions.
7. Check for convergence criterion.
8. EndDo
9. EndDo time loop

This specific scheme has often been advocated in the literature. For example, in the semi-conductor device simulation literature, it takes the name of Gummel's methods [20].

Many researchers observed that this form of block-relaxation schemes can be accelerated by some projection-type technique such as GMRES [19,21,23,24]. This is based on the observation made above that Algorithm 1 requires the Jacobian only in the form of matrix-vector products which can be evaluated with the simple formula (14). The resulting scheme is often referred to as a Nonlinear Krylov method.

The procedure can be described as follows. After each step in Algorithm 2, the iterates undergo a transformation which can be written as:

$$\begin{pmatrix} \mathbf{Y}_{new} \\ \mathbf{Z}_{new} \end{pmatrix} = \mathbf{M} \begin{pmatrix} \mathbf{Y} \\ \mathbf{Z} \end{pmatrix} \tag{17}$$

in which M is the nonlinear mapping which correspond to applying one step of the nonlinear Gauss-Seidel iteration. The iteration is attempting to solve the nonlinear equation:

$$\begin{pmatrix} \mathbf{Y} \\ \mathbf{Z} \end{pmatrix} - \mathbf{M} \begin{pmatrix} \mathbf{Y} \\ \mathbf{Z} \end{pmatrix} = 0 \ . \tag{18}$$

One can think of applying a Newton-like procedure based on Algorithm 1 for solving this system of equations. We will refer to this scheme as a Gauss-Seidel-Newton iteration.

3.3 Nonlinear Schur-complement algorithm

Upon eliminating the $\mathbf{Y}$ variable from the system (10), the equations to be solved can be restated in the following form

$$\Re(\mathbf{Z}(p_{fs}), t)) = 0 \tag{19}$$

The idea now is to attack the above problem as a nonlinear equation in $\mathbf{Z}$. It can be seen that $\Re = \mathbf{R}_2 - DA^{-1}\mathbf{R}_1$. Applying Newton's iteration to equations (19), leads to solving a linear system of the following form :

$$\Re'(\mathbf{Z})\delta\mathbf{Z} = -\Re(\mathbf{Z}(p_{fs})) \tag{20}$$

with $\Re' = B - DA^{-1}C$ the Jacobian of $\Re$. Thus, if the problem (19) has a solution then a solution to the original coupled fluid-structure problem can easily be obtained. When $\delta\mathbf{Z} = 0$, the fluid-structure interface does not move which implies that the fluid force does not change. However, the Jacobian $\Re'$ is not practically computable. Since the Nonlinear version of GMRES, Algorithm 1, requires only the action of the product of this Jacobian times a vector $\mathbf{V}$, the matrix $\Re'$ is actually not explicitly needed. Algorithm 1 can be used to solve the Schur complement problem (19). The products Jv in Line 6 of this algorithm, can be approximately evaluated by a simple forward finite scheme, analogous to (14):

$$\Re'(\mathbf{Z}) \cdot \mathbf{V} \approx \frac{\Re(\mathbf{Z} + \varepsilon\mathbf{V}) - \Re(\mathbf{Z})}{\varepsilon} \tag{21}$$

where ε is a small coefficient. The small-size linear system (20) (its size is actually the number of structural dry modes m) converges exactly in m iterations, even without any preconditioning. The most time consuming part of this algorithm is in the construction of the Krylov subspace. A significant saving can be obtained by freezing the Krylov subspace for a few time-iterations. However, in order to generate the Krylov directions, the pressure at the interface must be computed by the following computational steps :

Calculation of interface pressures :

1. Compute the coordinates of the structure corresponding to the perturbed modal coordinates $\mathbf{Z} + \varepsilon\mathbf{V}$.
2. Update the coordinates of the fluid nodes at the interface.
3. Update the mesh coordinates.
4. Update the fluid field.
5. Project the fluid pressure on the interface.

4 NUMERICAL RESULTS

Numerical simulations have been performed on the aeroelastic wing AGARD 445.6. This wing, has a symmetrical airfoil NACA 65A004 and a quarter-chord sweepback of 45 degrees, is immersed at a zero angle of attack in a transonic airflow. It has a mass of 0.1276 $slug$ (1.86227 kg), a Young's modulus of 4.7072×10^5 psi (3.2455×10^9 N/m^2), a Poisson ratio of 0.31 and a density of 0.8088 $slug/ft^3$ (416.86 kg/m^3). The structural domain is discretized by 1176 quadrilateral shell elements. The modal parameters are extracted with the commercial software ANSYS. The natural frequencies of the first five modes which are respectively 9.6, 39.4, 49.6, 96.1, 126.3 Hz and the modal vectors presented in Fig. 2 are in good agreement with the experimental results [4]. A coarse fluid mesh having 177042 linear tetrahedral elements and 37965 nodes is used. Since the strongest variation of the fluid variables occurs around the wing, the elements near the wing are much smaller than those in the rest of the fluid domain. There are 12921 fluid nodes and 25684 triangular elements on the wet surface of the wing on which slip boundary conditions are applied. Since the structural motion has no influence on the far-field boundaries, the flow is imposed as the incoming flow. The initial solution for the CFD solver is obtained by considering the wing as a rigid structure. The corresponding fluid configuration is considered as the initial state of the unsteady flow. From this state, a Dirac force is applied on the point located at the intersection between the wing tip and the leading edge. The Mach number of the oncoming flow is chosen as 0.96 in order to simulate the critical point of the transonic dip. The results of the flutter boundary prediction with our parallel code can be found in [25].

4.1 Numerical simulations with nonlinear Gauss-Seidel coupling algorithm

First, for the purpose of capturing the flutter dip with accuracy, a relatively small nondimensional time step of 0.1 which corresponds to a real time step of 2.01×10^{-4} *seconds* is used in the numerical simulations. At the aerodynamic pressure of 60 lb/ft^2 of the oncoming flow, the amplitudes of the lift and the generalized displacements(z_1, z_2) of the first two modes, which dominate the responses of the structural displacements, are constant and the critical flutter is captured. When the aerodynamic pressure of the oncoming flow increases to 61.3 lb/ft^2, the responses of the wing get increasing amplitudes and the wing is beyond the flutter point (Fig. 3). For the purpose of reducing the computing time, the numerical simulations with an increased nondimensional time step of 0.3 are performed, the flutter point is also captured at the aerodynamic pressure of 60 lb/ft^2. Figure 4 represents the time histories of the generalized displacement of the first two modes in comparison with another case with a higher aerodynamic pressure of 61.3 lb/ft^2.

At the flutter point with aerodynamic pressure of 60.0 lb/ft^2 and Mach number of 0.96, the damping coefficients are very small positives or negatives (see simulation (1) and (3) in Table 1), the coalesced frequency of 13.5 Hz (84.8 rad/s) of the first two modes is very close to the experimental one of 13.9 Hz (87.3 rad/s)[4]. The spectral distributions of the first two modes obtained with the Fast Discrete Fourier Transform confirm well the frequency coalescence (Fig. 5). The frequencies of the lift and the first two modes have practically the same value at the flutter point. This flutter aerodynamic pressure also agrees with the computational ones in [26,27]. When the aerodynamic pressure was increased to 61.3 lb/ft^2, the amplitudes of the generalized displacements of the first two modes start to increase and so does the difference of the frequencies of the oscillation. Table 1 summarizes the damping coefficients and the frequencies of the oscillation of the lift and the generalized displacements of the first two modes of the numerical simulations [28]. In simulation (1) and simulation (3) with aerodynamic pressure of 60.0 lb/ft^2, the damping coefficients are nearly zero and the frequencies are very close. The system reaches the flutter point (Fig.6).

In simulation (2) and simulation (4) with aerodynamic pressure of 61.3 lb/ft^2, the damping coefficients become negative and the difference of the frequencies of the first two modes starts to increase. The responses of the system indicate the flutter (Fig. 7). Simulation (3) and simulation (4) show that the nondimensional time step can be increased to 0.3, thus the computational speed is three times faster than simulation (1) and simulation (2).

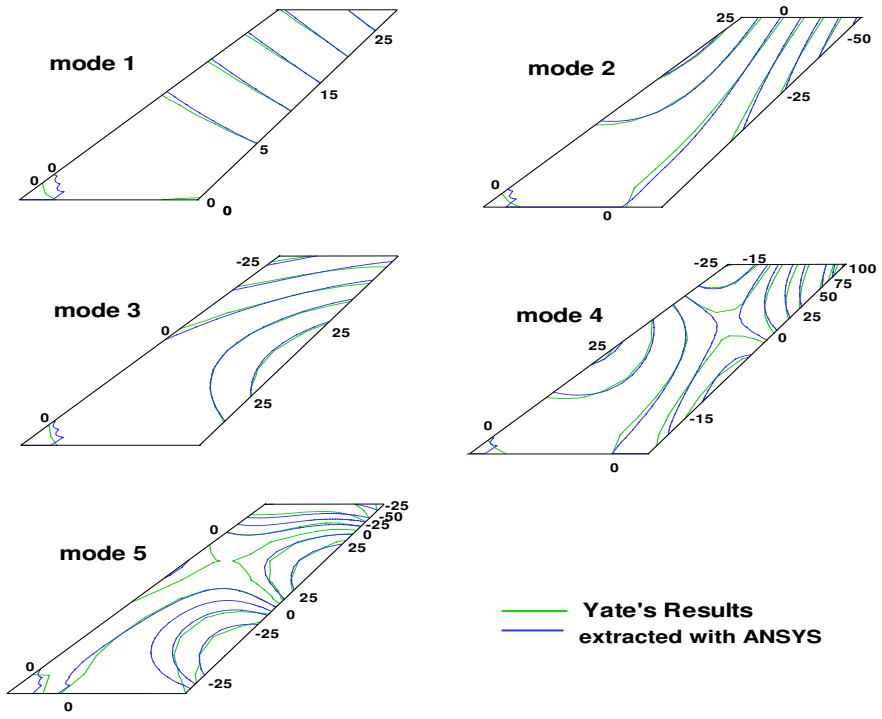

Fig. 2. Modal vectors of wing AGARD 445.6 extracted with ANSYS

4.2 Numerical simulations with nonlinear Schur-complement coupling algorithm

The Gauss-Seidel coupling algorithm gives satisfying results when the perturbation is small. However, this algorithm may have numerical instability and even may crash as the perturbation becomes strong. Schur-complement coupling algorithm can improve the robustness of the code. However, as the structural displacements increase, the linear mesh model is no longer stable. Figure 8 shows the comparisons of the generalized displacements of the first two modes obtained by Schur-complement algorithm with linear and nonlinear mesh models. From this figure we can see that the code gives the same results at the beginning of the simulations, but the simulation with linear mesh model stops at one instant due to the difficulty of convergence. Figure 9 shows the comparison of the numerical results obtained from the two nonlinear coupling algorithms at Mach number of 0.96 and aerodynamic pressure of 60 lb/ft^2. The strong force perturbation yields strong structural displacements which are 20 times larger than that of the test in the previous section. It is observed that the aeroelastic responses with Schur-complement coupling algorithm are more stable than those with the Gauss-Seidel coupling algorithm.

5 CONCLUSIONS

A nonlinear computational aeroelasticity model is developed using tight coupling algorithms. These coupling techniques reuse the developed linear CSD solver based on the modal analysis and the nonlinear CFD solver described by Euler equations. However, a matcher module and a mesh solver are required to match the CSD and CFD grids on the fluid-structure interface and to adapt the moving fluid boundaries. The use of the second order time discretization scheme and a nonlinear moving mesh model allows us to use large time steps for the staggered coupling algorithms. This model is applied to the standard aeroelastic wing AGARD 445.6 to predict the wing flutter, especially the

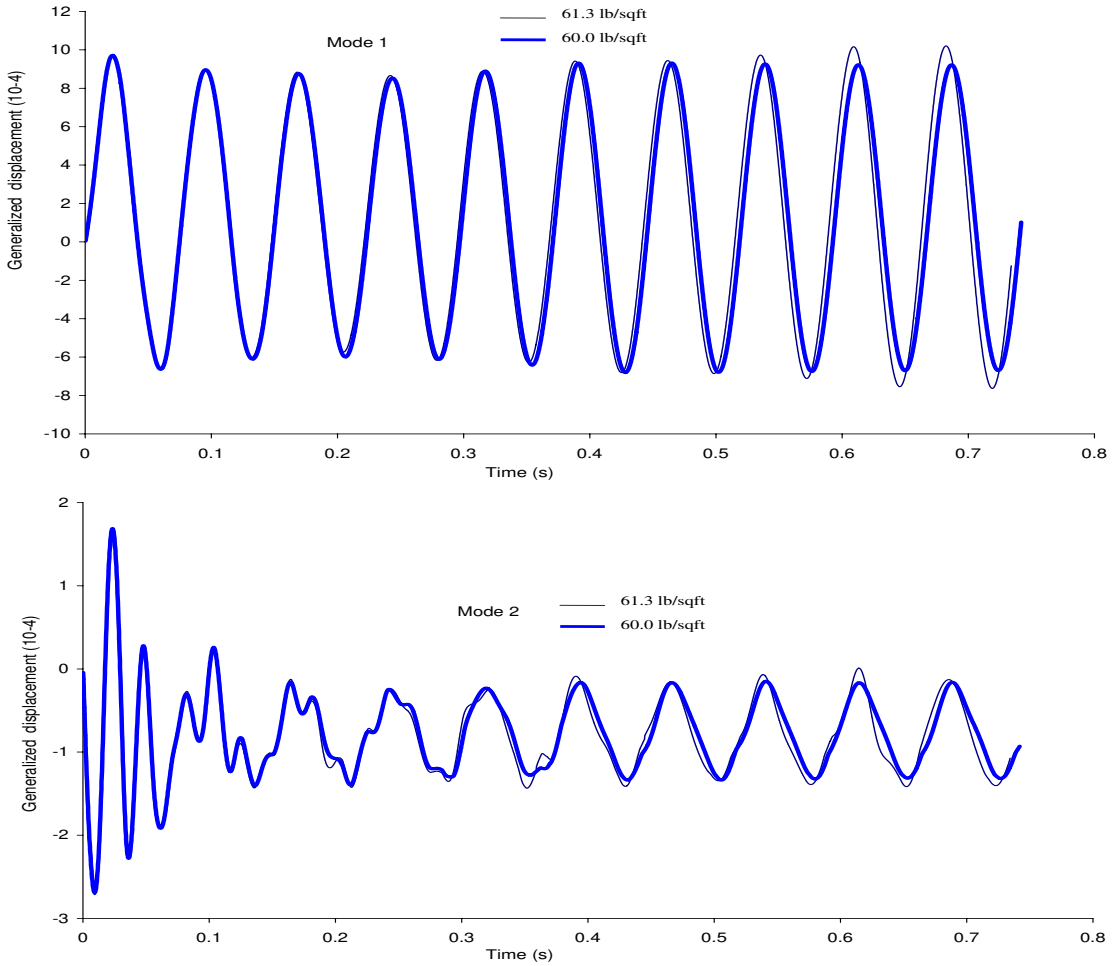

Fig. 3. Time history of the generalized displacements of the first two modes under a load perturbation with nondimensional time step of 0.1 at aerodynamic pressures 60 lb/ft^2 and 61.3 lb/ft^2

transonic dip. With a modest perturbation in transonic flows at Mach number 0.96, the results of the flutter simulation by the Gauss-Seidel coupling algorithm agree well with those in the references. The Schur-complement coupling algorithm improves the robustness of the code under stronger perturbation conditions.

References

[1] Dowell, E. H., 1995. A modern course in aeroelasticity (3rd rev. and enlarged ed.). Dordrecht, Pays-Bas : Kluwer Academic.

[2] Bisplinghoff, R. L., Ashley, H., 1962. Principles of Aeroelesticity. John Wiley and Sons, Inc.

[3] Fung, Y. C., 1969. An Introduction to the Theory of Aeroelasticity. Dover publications.

[4] Yates, E. C., Land, N. S., & Foughner, J. T., 1963. Measure and calculated subsonic and transonic flutter characteristics of a 45° sweptback wing planform in air and in Freon-12 in the Langley transonic dynamic tunnel. NASA Technical note, D-1616, March 1963.

[5] Dowell, E., Edwards, J., & Strganac, T., 2003. Nonlinear aeroelasticity. *Journal of Aircraft*, 40(5), 857-874.

[6] Shankar, V., & Ide, H., 1988. Aeroelastic computations of flexible configurations. *Computers & Structures*, 30(1-2), 15-28.

[7] Guruswamy, G. P., 1988. Interaction of fluids and structures for aircraft applications. *Computers & Structures*, 30(1-2), 1-13.

[8] Snyder, R. D., Scott, J. N., Khot, N. S., Beran, P. S., & Zweber, J. V., 2003. Predictions of store-induced limit-cycle oscillations using Euler and Navier-Stokes fluid dynamics. Paper presented at the 44th AIAA/ASME/ASCE/AHS/ASC Structures, Structural Dynamics, and Materials Conference, Apr 7-10 2003, Norfolk, VA, United States.

[9] Donea, J., 1982. An arbitrary Lagrangian-Eulerian finite element method for transient fluid-structure interactions. *Comput. Maths. Appl. Mech. Engrg* 33, 689-723.

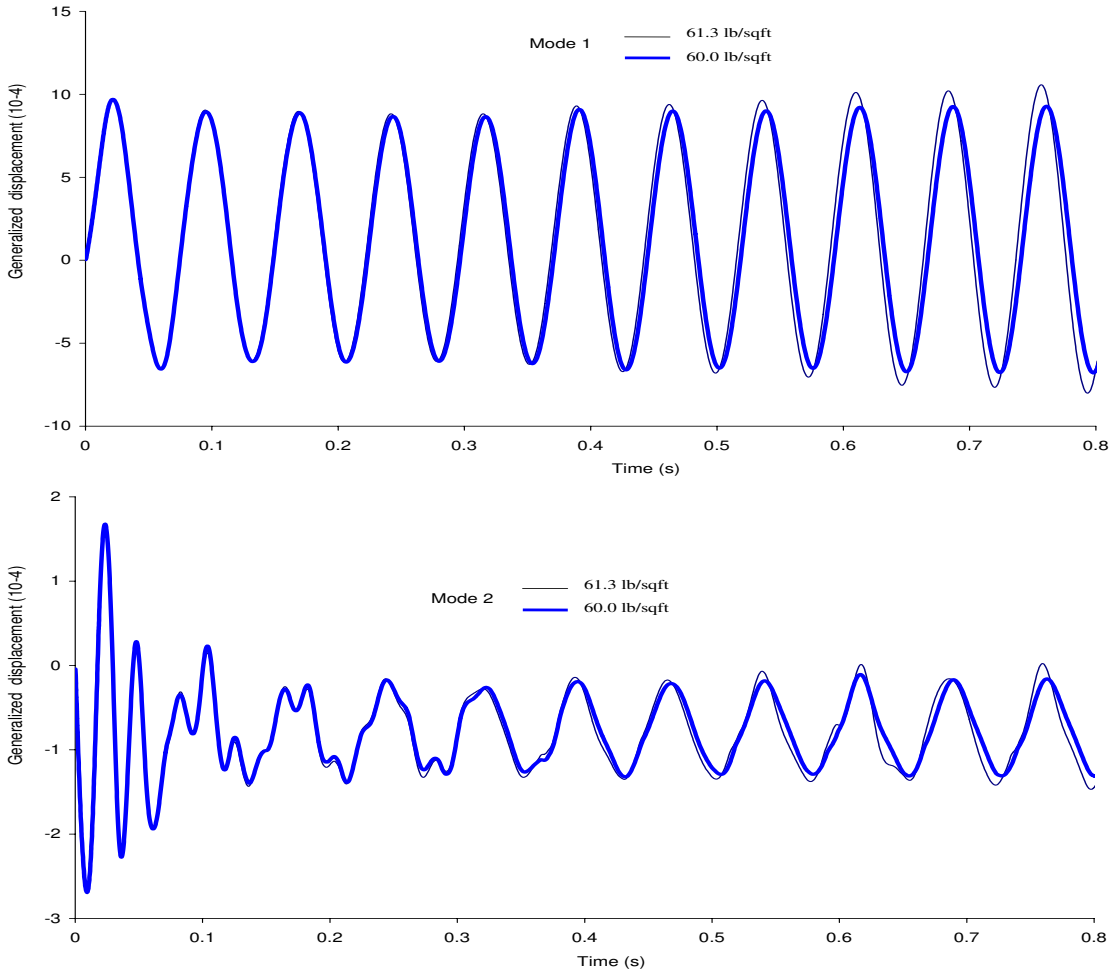

Fig. 4. Time history of the generalized displacements of the first two modes under a load perturbation with nondimensional time step of 0.3 at aerodynamic pressures 60 lb/ft^2 and 61.3 lb/ft^2

[10] Soulaimani, A., & Saad, Y., 1998. An Arbitrary Lagrangian Eulerian finite elemnt formulation for solving three-dimensional free surface flows. *Comput. Maths. Appl. Mech. Engrg*, 162, 79-106.

[11] Hughes, T.J.R., & Mallet, M., 1986. A new finite element formulation for computational fluid dynamics : III. The generalized streamline operator for multidimensional advective-diffusive systems. *Comput. Maths. Appl. Mech. Engrg*, 58, 305-328.

[12] Soulaimani, A., & Fortin, M., 1994. Finite element solution of compressible viscous flows using conservative variables. *Computer Methods in Applied Mechanics and Engineering*, 118(3-4), 319-350.

[13] Soulaimani, A., Saad, Y., & Mallet A., 2001. An edge based stabilized finite element method for solving compressible flows: formulation and parallel implementation. *Comput. Maths. Appl. Mech. Engrg*, vol. 190, 5867-5892.

[14] Soulainani, A., Ben Salah, N., & Saad, Y., 2002. Enhanced GMRES Acceleration Techniques for some CFD Problems.*International Journal of Computational Fluid Dynamics*, 16, 1-20.

[15] Farhat, C., Lesoinne, M., & Le Tallec, P., 1998. Load and motion transfer algorithms for fluid/structure interaction problems with non-matching discrete interfaces : Momentum and energy conservation, optimal discretization and application to aeroelasticity. *Computer Methods in Applied Mechanics and Engineering*, 157(1-2), 95-114.

[16] Lohner, R. et al. 1995. Fluid-Structure Interaction Using a Loose Coupling Algorithm and Adaptive Unstructured Grids. AIAA Paper 95-2259.

[17] Rifai, S.M., Johan, Z., Wang, W.P., Grisval, J.P., & Hughes, T.J.R. and Ferencz, R., 1999. Multiphysics simulation of flow-induced vibrations and Aeroelasticity on parallel computing platforms. *Comput. Maths. Appl. Mech. Engrg*, 174, 393-417.

[18] Soulamani, A., Feng, Z., & Ben Haj Ali, A., 2005. Solution techniques for multi-physics problems with application to computational nonlinear aeroelasticity. *Nonlinear Analysis*, 63(5-7), 1585-1595.

[19] Brown, P.N., & Saad, Y., 1990. Hybrid Krylov methods for nonlinear systems of equations. *SIAM J. Sci. Stat. Comp.*, 11:450-481.

[20] Kerkhoven, T., & Saad, Y., 1992. Acceleration techniques for decoupling algorithms in semiconductor simulation. *Num. Mat.*, 60:525-548.

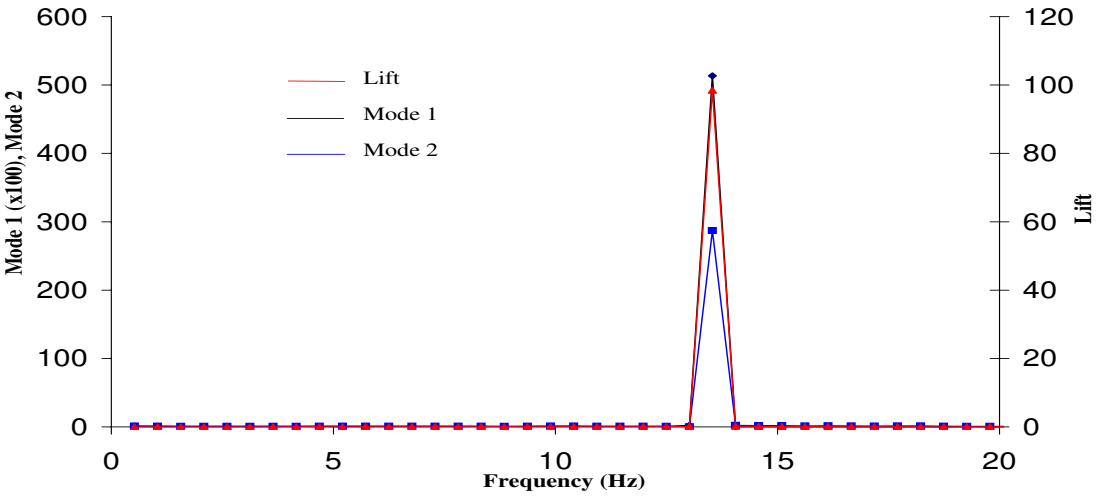

Fig. 5. Spectral distributions of the lift and the first two modes

Nondimensional time step		P_ref = 60 lb/sqft			P_ref = 61.3 lb/sqft		
	No. of test	simulation 1			simulation 2		
		lift	mode 1	mode 2	lift	mode 1	mode 2
	damping	0.00063	0.00063	0.00065	-0.0054	-0.00477	-0.00375
	Freq (Hz)	13.51	13.53	13.53	13.75	13.6	13.63
0.1	state	**calculated flutter point**			flutter with a small increasing amplitude		
	No. of simulation	simulation 3			simulation 4		
		lift	mode 1	mode 2	lift	mode 1	mode 2
	damping	-0.0002	-0.00017	-0.00025	-0.00537	-0.00475	-0.00667
	Freq (Hz)	13.52	13.52	13.52	13.58	13.58	13.6
0.3	state	**calculated flutter point**			flutter with a small increasing amplitude		

Table 1. Frequencies and damping coefficients of the oscillations of wing AGARD 445.6

[21] Wigton, L.B., Yu, D.P., & Young, N.J., 1985. GMRES acceleration of computational fluid dynamics codes. In *Proceedings of the 1985 AIAA conference, Denver 1985*, Denver.

[22] Ortega, J.M., & Rheinboldt, W.C., 1970. *Iterative solution of nonlinear equations in several variables.* Academic Press, New York.

[23] Chan, T.F., & Jackson, K.R., 1984. Nonlinearly preconditioned Krylov subspace methods for discrete Newton algorithms. *SIAM J. Stat. Scien. Comput.*, 7:533-542.

[24] Reisner, J., Mousseau, V., & Knoll, D., 2001. Application of the newton-krylov method to geophysical flows. *Monthly Weather Review*, 129:2404-2415.

[25] Soulamani, A., BenElHajAli, A., & Feng, Z., 2004. A Parallel-Distributed Approach for Multi-Physic Problems with Application to Computational Nonlinear Aeroelasticity. *the Canadian Aeronautics and Space Journal*, 50(4), p. 221-235.

[26] Gupta, K. K., 1996. Development of a finite element aeroelastic analysis capability. *Journal of Aircraft*, 33(5), 995-1002.

[27] Lesoinne, M., Sarkis, M., Hetmaniuk, U., & Farhat, C., 2001. A linearized method for the frequency analysis of three-dimensional fluid/structure interaction problems in all flow regimes. *Computer Methods in Applied Mechanics and Engineering*, 190(24-25), 3121-3146.

[28] Feng, Z., 2005. A nonlinear computational aeroelasticity model for aircraft wings. Ph.D. Thesis, École de technologie supérieure, University of Quebec, Montreal.

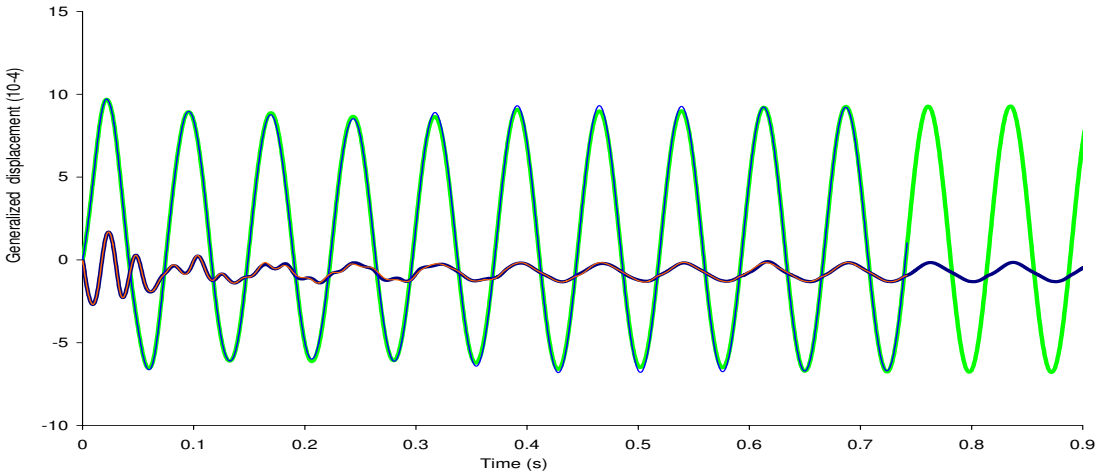

Fig. 6. Time history of the generalized displacements of the first two modes of the wing AGARD 445.6 under a load perturbation with nondimensional time step of 0.1 (blue and red curves for mode 1 and mode2 respectively) and 0.3 (green and black curves for mode 1 and mode2 respectively), aerodynamic pressure of $q = 60\ lb/ft^2$

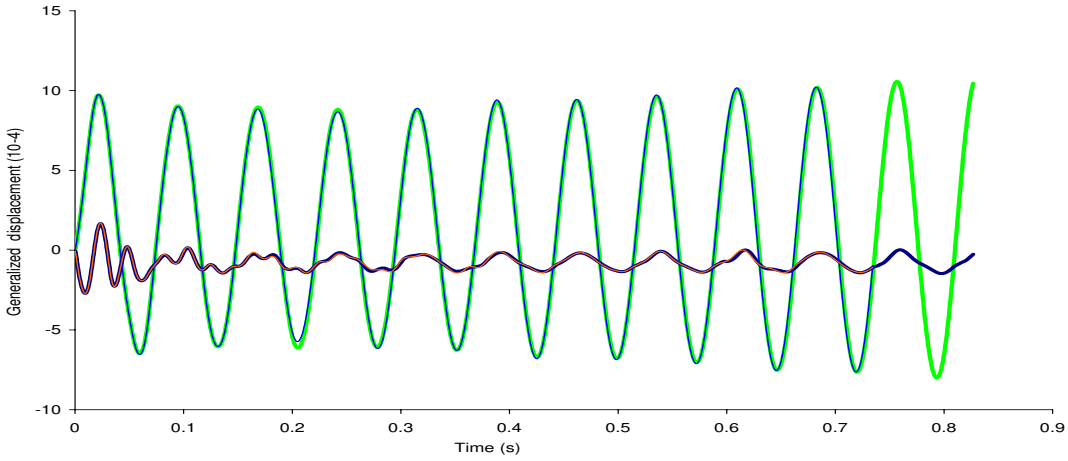

Fig. 7. Time history of the generalized displacements of the first two modes of the wing AGARD 445.6 under a load perturbation with nondimensional time step of 0.1 (blue and red curves for mode 1 and mode2 respectively) and 0.3 (green and black curves for mode 1 and mode2 respectively), aerodynamic pressure of $q = 61.3\ lb/ft^2$

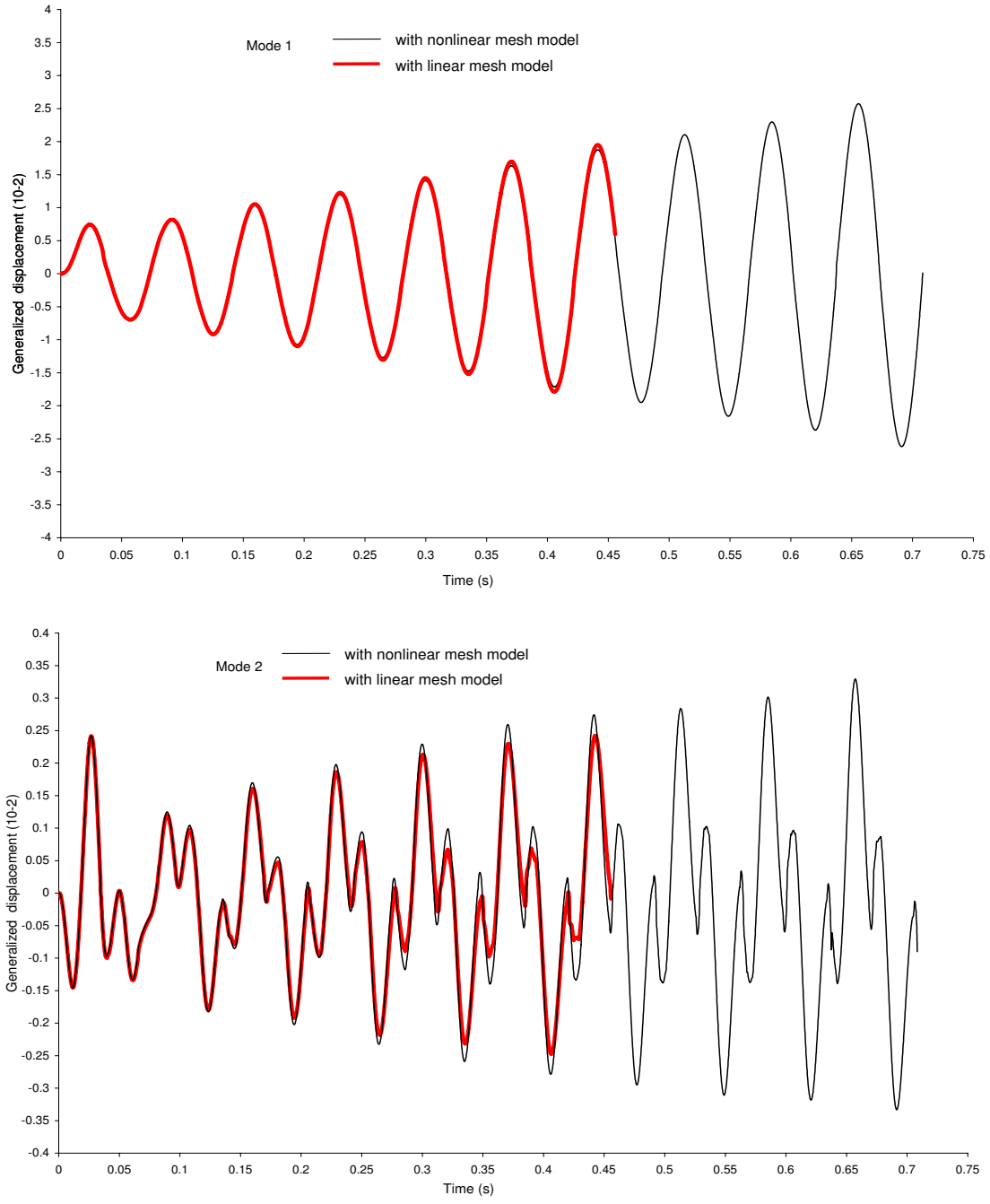

Fig. 8. Comparisons of the generalized displacements obtained by Schur-complement algorithm with linear and nonlinear mesh models of the first two modes under a load perturbation at aerodynamic pressures 60 lb/ft^2

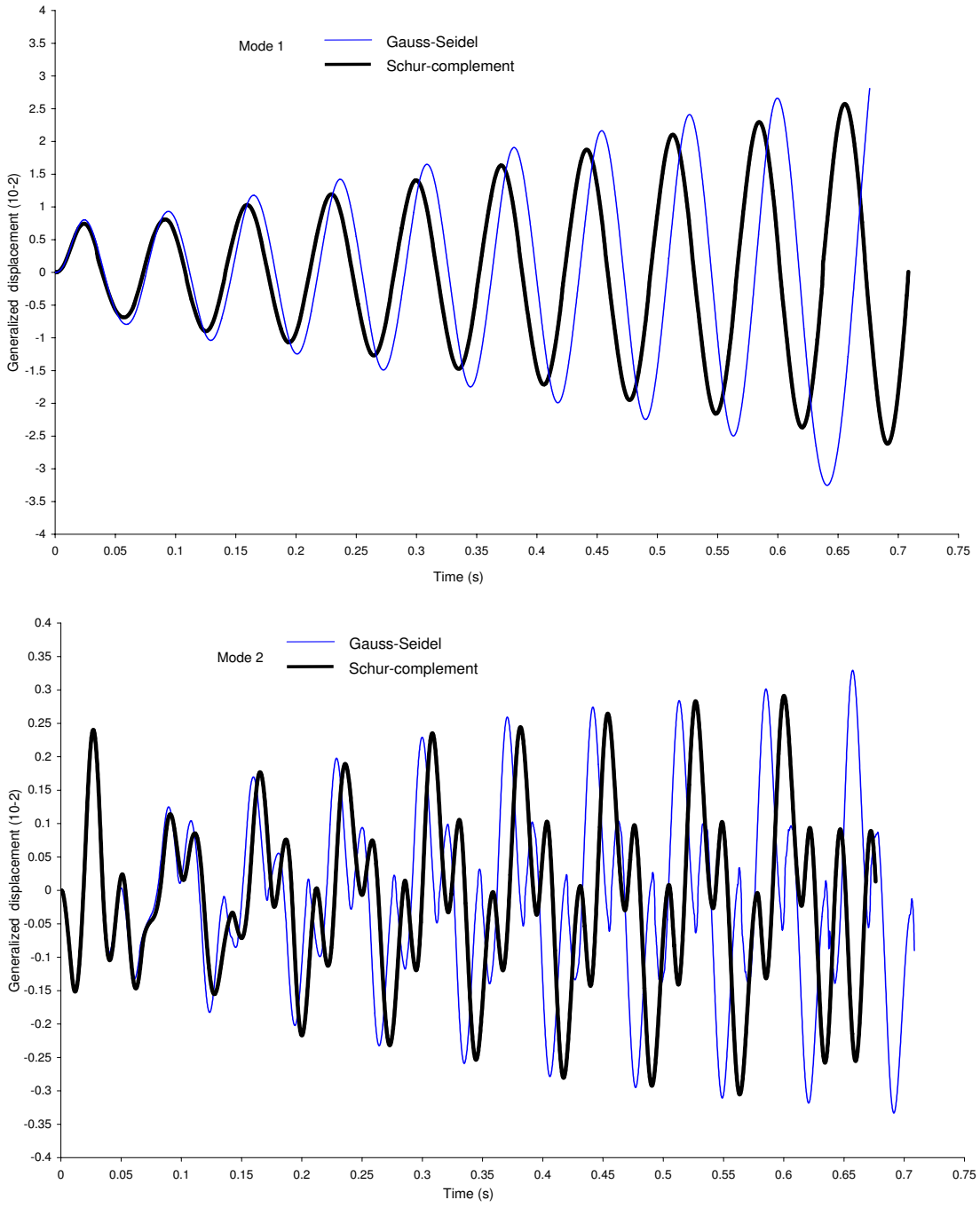

Fig. 9. Comparisons of the generalized displacements obtained by Gauss-Seidel and Schur-complement algorithms of the first two modes under a load perturbation at aerodynamic pressures 60 lb/ft^2